Open access • Journal Article • DOI:10.1243/03093240360713487

Stress analysis of V-notches with and without cracks, with application to foreign object damage — Source link

David Nowell, Daniele Dini, P. Duó

Institutions: University of Oxford

Published on: 01 Jan 2003 - Journal of Strain Analysis for Engineering Design (SAGE Publications)

Topics: Stress concentration, Stress intensity factor and Stress (mechanics)

Stress analysis of V-notches with and without cracks, with application to foreign object damage

D Nowell*, **D Dini** and **P Duó**
Department of Engineering Science, University of Oxford, UK

Abstract: Gas turbine engines can be subject to ingestion of small hard particles, leading to foreign object damage. This can take the form of sharp V-notches in the leading edge of blades and there is a need to predict the initiation and propagation behaviour of fatigue cracks growing from the base of the notch. The notch geometry is quite extreme and is not normally covered in standard references for notch stress concentration factors. Similarly, stress intensity factor solutions for this geometry are not widely available. This paper uses the dislocation density approach to solve the two-dimensional elastic problem of a V-notch with a radiused root. Stress concentration factors are found for the notch itself, and stress intensity factors are determined for cracks growing away from the notch for cases of applied and residual stress distributions. Comparisons are made with existing notch solutions from the literature.

Keywords: notches, cracks, stress concentration factors, stress intensity factors, foreign object damage, residual stress

NOTATION

a	crack length
b	notch depth
b_x, b_y	Burgers vector components
B_x, B_y	Burgers vector densities
G	kernel function
K_{I}	stress intensity factor
K_t	stress concentration factor
N	number of points in the discretization
r	ordinate along crack
s	distance from the surface to the root along the notch boundary
t	ordinate along the notch boundary
u	normalized ordinate along the notch boundary
u_i	integration point
v_k	collocation point
w	weight function
x, y	Cartesian coordinates
$x_{\mathrm{d}}, y_{\mathrm{d}}$	dislocation position
ε	small distance
θ	semi-angle of the notch
κ	Kolosov's constant
μ	shear modulus
ν	Poisson's ratio
ρ	notch root radius
σ_0	stress remote from the notch
σ^{d}	stress due to dislocations
$\sigma_{\mathrm{NN}}, \sigma_{\mathrm{NT}}$	tractions on the crack or notch boundary
ϕ	rotation angle in stress transformation
Φ	bounded part of the dislocation density distribution

The MS was received on 29 January 2003 and was accepted after revision for publication on 12 June 2003.
* *Corresponding author: Department of Engineering Science, University of Oxford, Parks Road, Oxford OX1 3PJ, UK.*

1 INTRODUCTION

Gas turbine engines are used to power many civil and military aircraft. The high airflow required results in a powerful suction effect, which can cause the engine to ingest solid objects that may cause damage to the engine. These objects generally fall into two categories:

(a) soft objects such as birds or ice and
(b) small hard objects such as stones and rivets.

Ingestion of objects in the second category is normally termed 'foreign object damage' (FOD). Such objects typically cause damage to the leading edge of the fan or compressor blades [**1**]. The damage is often quite small, taking the form of a 'nick' in the leading edge, so that it can be difficult to pick up during a simple visual inspection of the engine prior to flight. The presence of the FOD will reduce the fatigue strength of the blade

and can lead to failure under normal levels of blade vibration. In recent years there has been increasing interest in predicting the effect of FOD on blade fatigue strength [2]. The objectives of this work are to provide tools which will enable the assessment of damaged blades in service and the development of FOD-resistant designs of blade. FOD observed in service can vary considerably in size and geometry, due to the range of objects ingested and the widely varying impact speeds, location and orientation [1]. Experimental work to reproduce this type of damage in the laboratory has been undertaken by a number of workers (see, for example, references [3] and [4]). A range of projectiles has been used, but there is widespread agreement that the largest reduction in fatigue strength is found from sharp V-notches in the leading edge. Figure 1 shows typical damage created by a laboratory gas gun using hardened steel cubes [3].

Alongside the experimental work in this area, attempts have been made to predict the loss of fatigue strength caused by FOD [3, 5]. In order to carry out a fatigue assessment it is necessary to know the stresses in the neighbourhood of an FOD notch and, if a fracture mechanics approach is to be used, stress intensity factors for cracks emanating from the notch. The required tools are, however, not readily available in the literature. Sharp FOD notches have higher stress concentration (K_t) values than most features that would be designed into a component and appropriate K_t solutions do not appear in standard reference works [6]. Similar remarks apply to the case where a crack is present. Again standard reference works [7] give very few solutions which apply to sharp V-notches. Clearly it would be possible to pursue a solution based on finite element procedures, but the overall requirement suggests that a range of geometries and crack lengths will need to be investigated. It may also be necessary to include the effects of residual stress, either from pre-existing surface treatment or arising from the impact itself. It is appropriate, therefore, to pursue a more specialized approach that will be capable of investigating a range of geometries, parametrically described. The technique chosen here is based on the dislocation density method [8, 9] which has been found to be effective for two-dimensional cracks and slots. In effect the method may be considered as a displacement discontinuity boundary element method, employing a small number of high-order elements.

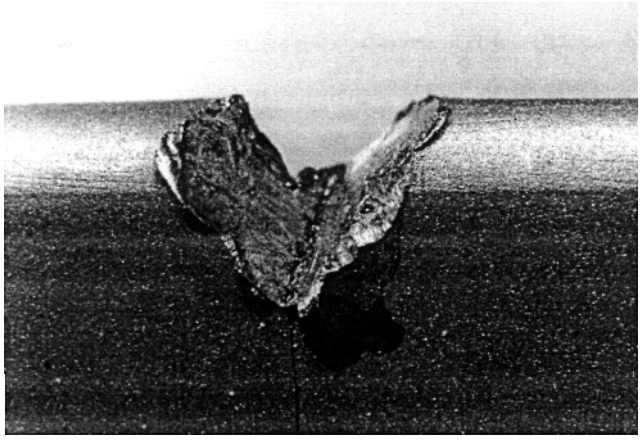

Fig. 1 Typical FOD notch on the leading edge of a compressor blade

2 NOTCHES WITHOUT CRACKS

2.1 Formulation

The general geometry of the notch that is to be analysed is shown in Fig. 2a. The notch depth is b, and the notch angle is 2θ. The root of the notch has a radius of ρ. In the case of a real FOD notch, the boundaries of the blade (other than the leading edge itself) will be remote from the notch. Therefore a notch in a half-plane (i.e. with a single free boundary) was chosen for consideration. In this case, the notch can be uniquely described by θ and ρ/b. As stated above, the analysis employed will be two dimensional and also elastic material behaviour will be assumed. It is recognized that there may be some macroscopic cyclic plasticity during fatigue loading of a damaged component, but an elastic analysis would still appear to be an appropriate place to start. If the notch is loaded by a stress in the y direction, symmetry will apply and the problem can be simplified by considering only half of the notch (Fig. 2b). Simple geometry shows that the half-length of the free boundary of the notch, s, is given by

$$\frac{s}{b} = \frac{1}{\cos\theta} + \frac{\rho}{b}\left(\tan\theta + \frac{\pi}{2} - \theta - \frac{1}{\cos\theta}\right) \tag{1}$$

The case where a uniform far-field stress σ_0 is applied parallel to the free surface (i.e. in the y direction) is considered. A point on the boundary of the notch will experience an unsatisfied normal traction σ_{NN} and an unsatisfied shear traction σ_{NT} given by the two-dimensional stress transformation equations as

$$\sigma_{NN} = \frac{\sigma_0}{2}[1 + \cos(2\phi)] \tag{2}$$

$$\sigma_{NT} = \frac{\sigma_0}{2}\sin(2\phi) \tag{3}$$

where ϕ is the angle between the local boundary of the notch and the y axis. It is noted that $\phi = -\theta$ on the straight part of the notch boundary and varies from $-\theta$ to $-\pi/2$ over the curved portion at the root. These unsatisfied tractions are to be met by installing arrays of displacement discontinuities (or dislocations) along the boundary of the notch. The stress field due to a

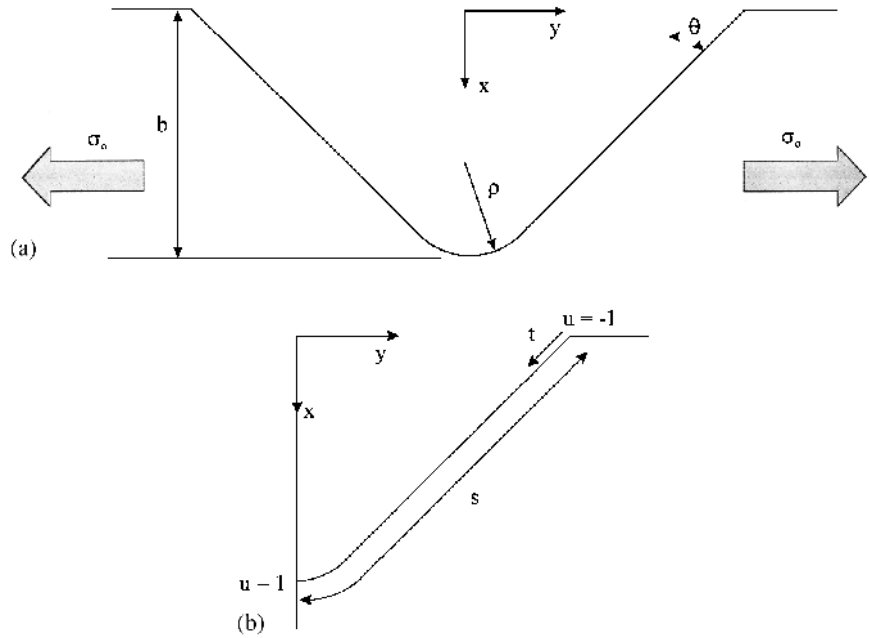

Fig. 2 (a) Geometry of an idealized two-dimensional V-notch; (b) half-problem analysed, taking advantage of symmetry

dislocation positioned at (x_d, y_d) with Burgers vector components b_x in the x direction and b_y in the y direction (Fig. 3) is first described. The stress components at a remote point (x, y) due to the Burgers vector component b_k are given by

$$\sigma^{d}_{ijk} = \frac{\mu}{\pi(\kappa+1)} b_k G_{kij}(x, x_d, y - y_d) \tag{4}$$

where μ is the shear modulus and κ is Kolosov's constant [equal to $(3-4\nu)$ in plane strain and $(3-\nu)/(1+\nu)$ in plane stress, where ν is Poisson's ratio]. The functions G_{kij} are simple algebraic functions, given in reference [**9**].

Rather than installing discrete dislocations it is arranged to install continuous distributions of Burgers vector densities B_x and B_y along the boundary of the notch $(0 < t < s)$ (Fig. 2b). The total stress at a point (x, y) due to these distributions will therefore be

$$\sigma^{d}_{ij} = \frac{\mu}{\pi(\kappa+1)} \int_0^s B_x G_{xij}(x, x_d, y - y_d)\,\mathrm{d}t + \frac{\mu}{\pi(\kappa+1)} \int_0^s B_y G_{yij}(x, x_d, y - y_d)\,\mathrm{d}t \tag{5}$$

In order to take account of symmetry it is recognized that there will also need to be distributions on the left-hand side of the notch, with densities given by

$$B_x(x_d, -y_d) = -B_x(x_d, y_d) \tag{6}$$

and

$$B_y(x_d, -y_d) = B_y(x_d, y_d) \tag{7}$$

so that the total stress due to distributions on both sides

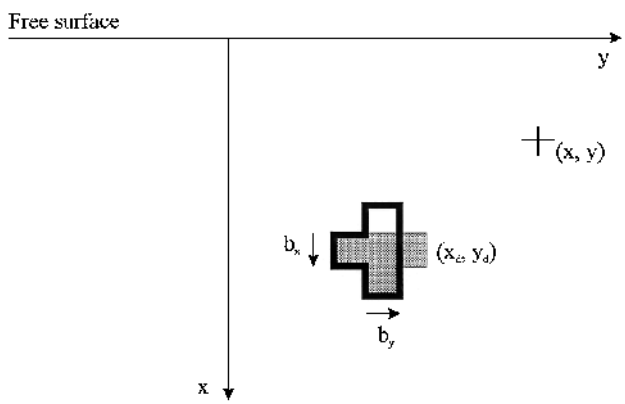

Fig. 3 A dislocation in a half-plane with Burgers vector strengths b_x and b_y in the x and y directions respectively

of the notch may now be expressed as

$$\sigma_{ij}^{\mathrm{d}} = \frac{\mu}{\pi(\kappa+1)} \int_0^s B_x G'_{xij}(x, x_{\mathrm{d}}, y - y_{\mathrm{d}})\,\mathrm{d}t + \frac{\mu}{\pi(\kappa+1)} \int_0^s B_y G'_{yij}(x, x_{\mathrm{d}}, y - y_{\mathrm{d}})\,\mathrm{d}t \quad (8)$$

where

$$G'_{xij}(x, x_{\mathrm{d}}, y - y_{\mathrm{d}}) = G_{xij}(x, x_{\mathrm{d}}, y - y_{\mathrm{d}}) - G_{xij}(x, x_{\mathrm{d}}, y + y_{\mathrm{d}}) \quad (9)$$

and

$$G'_{yij}(x, x_{\mathrm{d}}, y - y_{\mathrm{d}}) = G_{yij}(x, x_{\mathrm{d}}, y - y_{\mathrm{d}}) + G_{yij}(x, x_{\mathrm{d}}, y + y_{\mathrm{d}}) \quad (10)$$

It is convenient to express these stresses in components normal and tangential to the notch surface so that

$$\sigma_{\mathrm{NN}}^{\mathrm{d}} = \frac{\mu}{\pi(\kappa+1)} \int_0^s B_x G'_{x\,\mathrm{NN}}(x, x_{\mathrm{d}}, y, y_{\mathrm{d}}, \phi)\,\mathrm{d}t + \frac{\mu}{\pi(\kappa+1)} \int_0^s B_y G'_{y\,\mathrm{NN}}(x, x_{\mathrm{d}}, y, y_{\mathrm{d}}, \phi)\,\mathrm{d}t \quad (11)$$

and

$$\sigma_{\mathrm{NT}}^{\mathrm{d}} = \frac{\mu}{\pi(\kappa+1)} \int_0^s B_x G'_{x\,\mathrm{NT}}(x, x_{\mathrm{d}}, y, y_{\mathrm{d}}, \phi)\,\mathrm{d}t + \frac{\mu}{\pi(\kappa+1)} \int_0^s B_y G_{y\,\mathrm{NT}}(x, x_{\mathrm{d}}, y, y_{\mathrm{d}}, \phi)\,\mathrm{d}t \quad (12)$$

where

$$G_{k\,\mathrm{NN}} = \frac{G'_{kxx} + G'_{kyy}}{2} - \frac{G'_{kxx} - G'_{kyy}}{2}\cos(2\phi) - G'_{kxy}\sin(2\phi) \quad (13)$$

$$G_{k\,\mathrm{NT}} = \frac{G'_{kyy} - G'_{kxx}}{2}\sin(2\phi) + G'_{kxy}\cos(2\phi) \quad (14)$$

It is now noted that the stresses due to the dislocation distributions must cancel the original unsatisfied tractions along the surface of the notch so that

$$\sigma_{\mathrm{NN}} + \sigma_{\mathrm{NN}}^{\mathrm{d}} = 0, \qquad 0 < t < s \quad (15)$$

and

$$\sigma_{\mathrm{NT}} + \sigma_{\mathrm{NT}}^{\mathrm{d}} = 0, \qquad 0 < t < s \quad (16)$$

Substitution of equations (2) and (11) into equation (15) and of equations (3) and (12) into equation (16) gives two simultaneous equations in the unknown Burgers vector densities B_x and B_y. It should be noted that these display Cauchy singularities because of the nature of the influence functions G. Standard numerical techniques are available for the solution of this type of problem. Full details have been given in reference [**8**] or [**10**], and only a brief outline will be given here. The steps are as follows:

1. Normalize the limits of integration to ± 1 by an appropriate change of variables. In this case $u = -1$ corresponds to $t = 0$ and $u = 1$ corresponds to $t = s$, so that $u = 2t/s - 1$.
2. Consider the behaviour of the unknown function at the ends of the interval. Here we expect bounded and non-zero behaviour at both ends of the interval $t = 0$, s, except for B_x at $t = s$, where the function will be bounded and zero [equation (6)]. Gauss–Jacobi or Gauss–Chebyshev quadrature is appropriate for Cauchy-singular integral equations and this offers the option of bounded and zero or $r^{-0.5}$ behaviour at each end point [**10**]. It has been shown that incorporation of a stronger singularity than that present is generally satisfactory [**11**], and here a fundamental function giving $r^{-0.5}$ behaviour at $t = s$, with bounded and zero behaviour at $t = 0$, will be chosen. This choice will also be appropriate later, when a crack is added, emanating from the root of the notch. It will also be shown to give acceptable behaviour for the case without a crack. Accordingly B_k is modelled as the product of a bounded function $\Phi_k(t)$ and a weight function $w(t)$ with

$$w(t) = \sqrt{\frac{1+t}{1-t}} \quad (17)$$

so that

$$B_k = \Phi_k(t)\sqrt{\frac{1+t}{1-t}} \quad (18)$$

3. Gauss–Jacobi integration is now applied to reduce the integral equations to a series of $2N$ simultaneous linear equations, enforced at N collocation points:

$$\sigma_{\mathrm{NN}} + \frac{\mu}{\pi(\kappa+1)} \sum_{i=1}^{N} \frac{2\pi(1+u_i)}{2N+1} G'_{x\,\mathrm{NN}}(u_i, v_k)\Phi_x(u_i) + \frac{\mu}{\pi(\kappa+1)} \sum_{i=1}^{N} \frac{2\pi(1+u_i)}{2N+1} G'_{y\,\mathrm{NN}}(u_i, v_k)\Phi_y(u_i) = 0 \quad (19)$$

and

$$\sigma_{\mathrm{NT}} + \frac{\mu}{\pi(\kappa+1)} \sum_{i=1}^{N} \frac{2\pi(1+u_i)}{2N+1} G'_{x\,\mathrm{NT}}(u_i, v_k)\Phi_x(u_i) + \frac{\mu}{\pi(\kappa+1)} \sum_{i=1}^{N} \frac{2\pi(1+u_i)}{2N+1} G'_{y\,\mathrm{NT}}(u_i, v_k)\Phi_y(u_i) = 0 \quad (20)$$

where the integration points u_i are given by

$$u_i = \cos\left(\frac{2i-1}{2N+1}\pi\right), \qquad i = 1, 2, \ldots, N \tag{21}$$

and the collocation points v_k by

$$v_k = \cos\left(\frac{2k}{2N+1}\pi\right), \qquad i = 1, 2, \ldots, N \tag{22}$$

For acceptable accuracy, N is usually chosen in the range $50 < N < 100$. The simultaneous equations may be solved by an appropriate procedure (e.g. LU decomposition). The results presented in this paper were obtained with $N = 70$.

4. Once $\Phi_x(u_i)$ and $\Phi_y(u_i)$ have been determined, stress components due to the dislocations at a general point (x, y) in the half-plane may be found using similar expressions to equations (19) and (20), specifically

$$\sigma_{ij}^{d} = \frac{\mu}{\pi(\kappa+1)} \sum_{i=1}^{N} \frac{2\pi(1+u_i)}{2N+1} G'_{xij}(u_i, x, y)\Phi_x(u_i) + \frac{\mu}{\pi(\kappa+1)} \sum_{i=1}^{N} \frac{2\pi(1+u_i)}{2N+1} G'_{y\,\mathrm{NT}}(u_i, x, y)\Phi_y(u_i) \tag{23}$$

It should be noted that in this case the integrals are not Cauchy provided that (x, y) does not lie on the boundary of the notch. The validity of the expression is not, therefore, limited to specific collocation points. To evaluate the total stress state it is merely necessary to add the original stress state in the absence of the notch, in this case $\sigma_{yy} = \sigma_0$.

2.2 Results

It is appropriate to start by examining the validity of the assumptions regarding the end-point behaviour of the dislocation density. Figure 4 shows normalized B_x and B_y as functions of position t/s for a number of sample cases. It may be seen that, apart from the final integration points, a smooth representation of the functions is obtained. Thus, it may be concluded that precise modelling of end-point behaviour is not necessary in this case. It is also noted that increasing the tip radius gives lower density curves in the neighbourhood of the notch tip. Figure 5 gives the variation in the σ_{yy} stress component along $y = 0$, i.e. the vertical line passing through the root of the notch for $\theta = 45°$ and a number of different root radii b/ρ. It will be noted that the stress component is effectively zero for $x < b$, corresponding to the portion of the half-plane 'removed' to create the notch by clearing the boundaries of tractions. For $x > b$, stresses are close to the far-field value σ_0 remote from the notch and increase to a value equal to $K_t\sigma_0$ at the notch root, where K_t is the elastic stress concentration factor for the notch. Some care is necessary in evaluating K_t; the numerical scheme will result in a stress field which is continuous, since no discrete dislocations are employed. In practice, there should be a discontinuity in the σ_{yy} stress component between 0 at $x = b - \varepsilon$ and $K_t\sigma_0$ at $x = b + \varepsilon$, where ε is

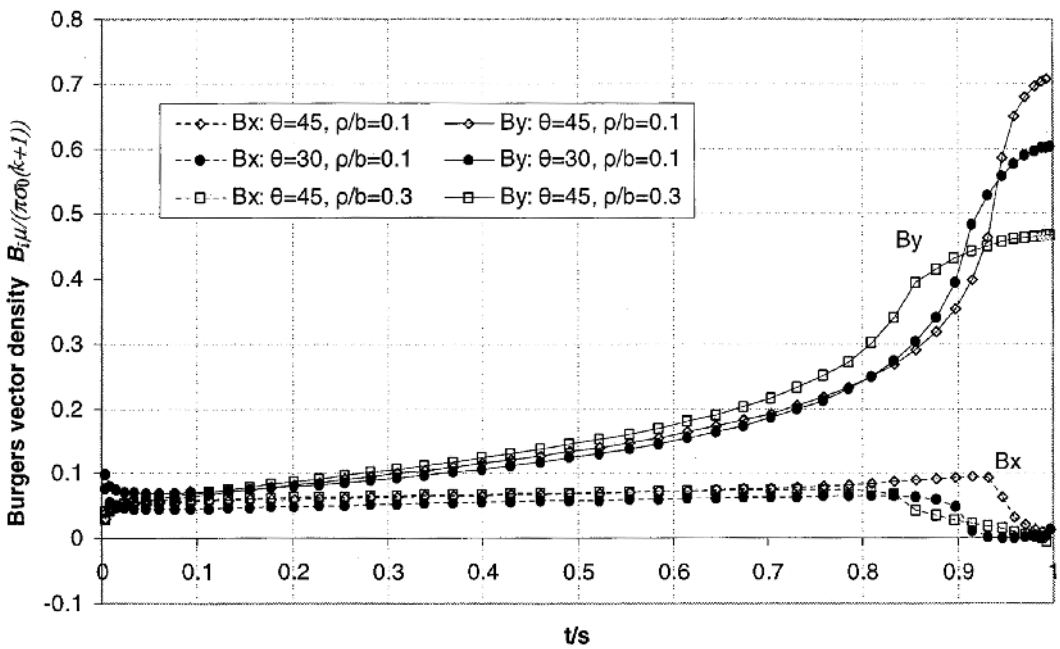

Fig. 4 Variation in Burgers vector density for a 45° notch with $\rho/b = 0.5$

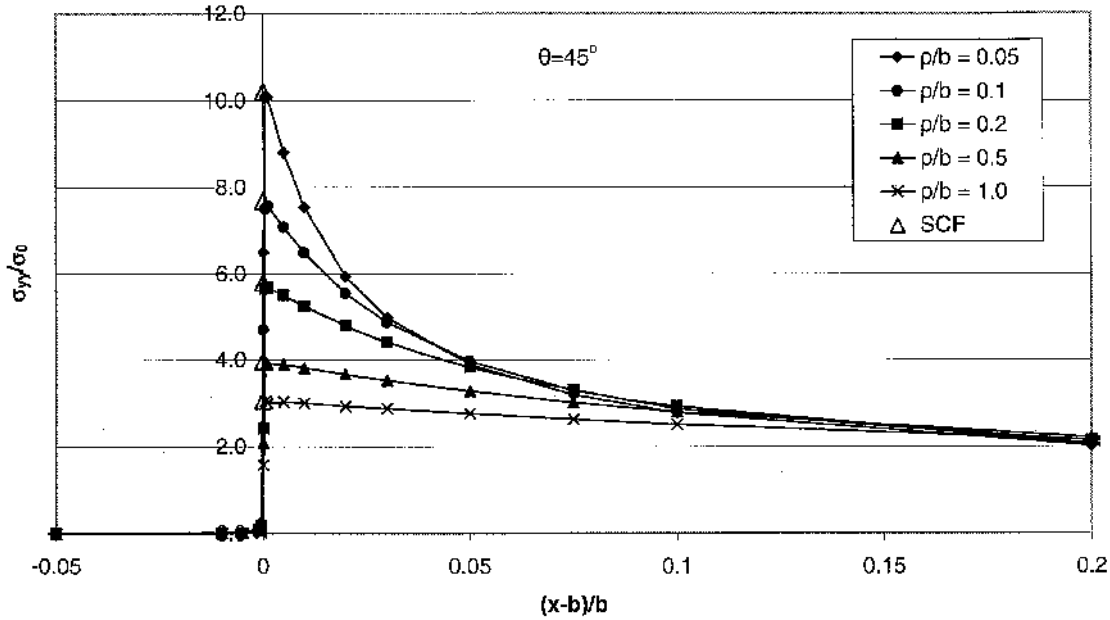

Fig. 5 σ_{yy} stress component along $y = 0$, $\theta = 45°$ (SCF, stress concentration factor)

a small distance. This discontinuity is not precisely captured by the scheme, although Fig. 5 shows that the approximation is very good. Simply evaluating the stress at $x = b$ will give a value which is between 0 and $K_t\sigma_0$. A satisfactory approach for determining K_t is to use linear extrapolation from two points close to $x = b$. Values of K_t given here were obtained by extrapolation using $x = b + 0.05\rho$ and $x = b + 0.01\rho$. Figure 5 shows that the stresses are strongly dependent on ρ close to the notch root but are almost independent of ρ further away. This point is emphasized if the stresses are plotted using a different normalization (Fig. 6). Here $\sigma_{yy}/K_t\sigma_0$ is plotted against $(x - b)/\rho$. It may be seen that the response close to the notch may be described by ρ alone; i.e. the stresses are independent of b, other than through the influence of ρ/b on K_t.

Figure 7 shows the variation in the σ_{yy} stress along $y = 0$ for $\rho/b = 0.2$ and several different notch angles θ. It will be seen that the influence of notch angle at this value of ρ/b is very small for $\theta < 45°$. The implication of

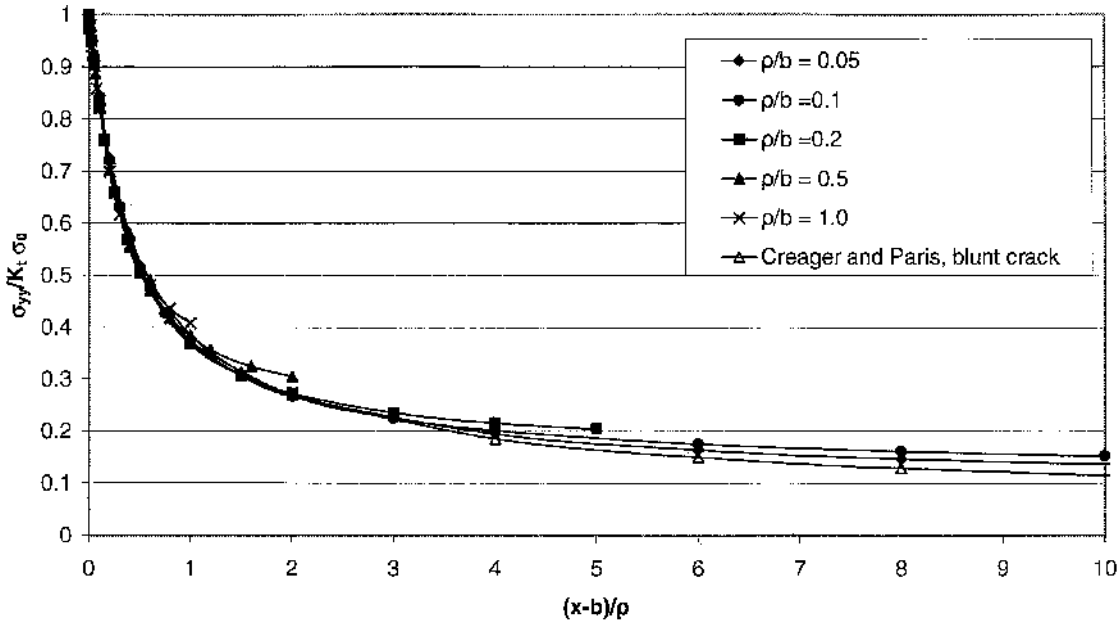

Fig. 6 σ_{yy} stress component plotted normalized with respect to K_t and ρ to show the dependence on the notch root radius

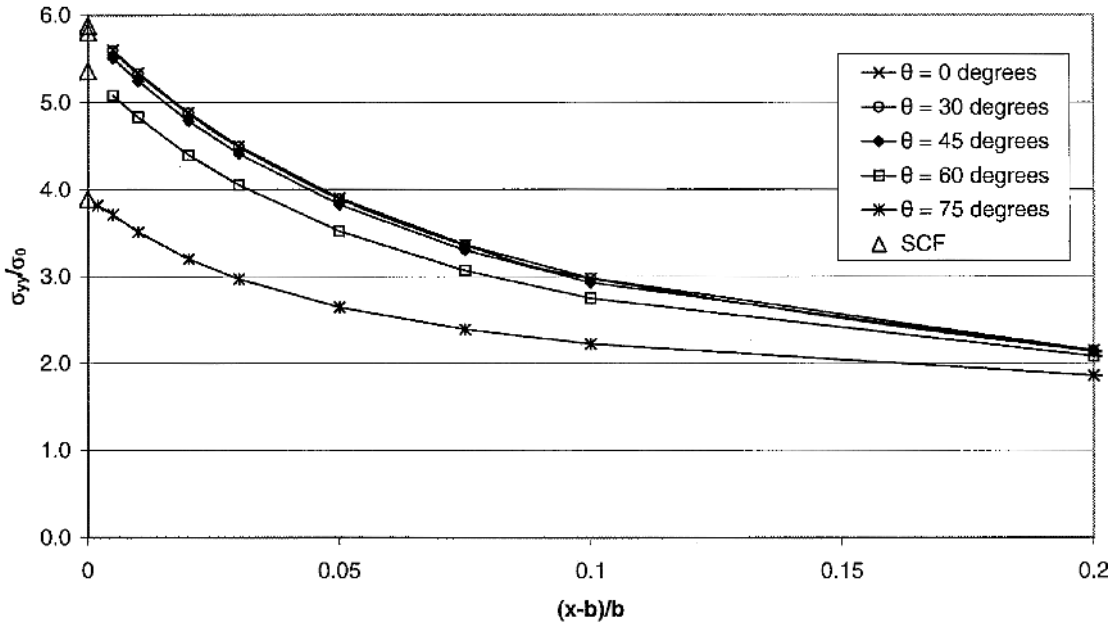

Fig. 7 Effect of θ on the σ_{yy} stress component along $y = 0$, $\rho/b = 0.2$ (SCF, stress concentration factor)

this observation is that, as far as this stress component is concerned, notch angles less than 45° may be treated as if they were a blunt crack with the same depth and root radius. A comprehensive set of results is presented in Table 1, where values of K_t are given for a range of values of θ and ρ/b.

The same information is presented graphically in Fig. 8, where it can be seen that the sensitivity of K_t to θ increases as ρ/b is decreased. It should be noted that $\rho/b = 1.0$, $\theta = 0°$, corresponds to a semicircular notch, for which the accepted value of K_t is around 3.0. Roarke and Young [**6**] gave values of K_t for this configuration: 2.988 for a single notch in a wide plate, and 3.065 for two opposite notches in a wide plate. It will be seen that the current method gives a result within this range. Finally, it is possible to obtain information for the stresses anywhere around the notch, and not just along $y = 0$, although this is the principal region of interest for the current paper, where the interest lies in cracks initiating and growing along this line. Figure 9 shows contours of σ_{yy}/σ_0 around the notch for $\theta = 45°$, and $\rho/b = 0.5$. The concentration of contours close to some points on the notch boundary is a result of the difficulty of evaluating the stress correctly close to the dislocation distribution but away from a collocation point.

2.3 Comparison with classical methods

In order to evaluate the accuracy of the solution, comparisons with classical solutions [**12**–**15**] of linear elastic stress analysis of notches were carried out. However, due to space consideration, only the comparison with the most general solution developed by Filippi *et al.* [**16**] will be presented here. The analytical solution proposed in reference [**16**] is an improvement of the previous solution developed in reference [**15**] and it is based on the Kolosoff–Muskhelishvili potential functions method, providing good accuracy in calculating the stress field in the

Table 1 Variation in K_t with θ and ρ/b

	K_t				
θ (deg)	$\rho/b = 0.05$	$\rho/b = 0.1$	$\rho/b = 0.2$	$\rho/b = 0.5$	$\rho/b = 1.0$
0	10.750	8.044	5.878	3.988	3.058
15	10.654	8.032	5.877	3.987	3.058
30	10.569	7.979	5.875	3.987	3.058
45	10.199	7.694	5.803	3.969	3.055
60	9.216	6.708	5.361	3.828	3.009
75	6.403	5.194	3.894	3.133	2.643

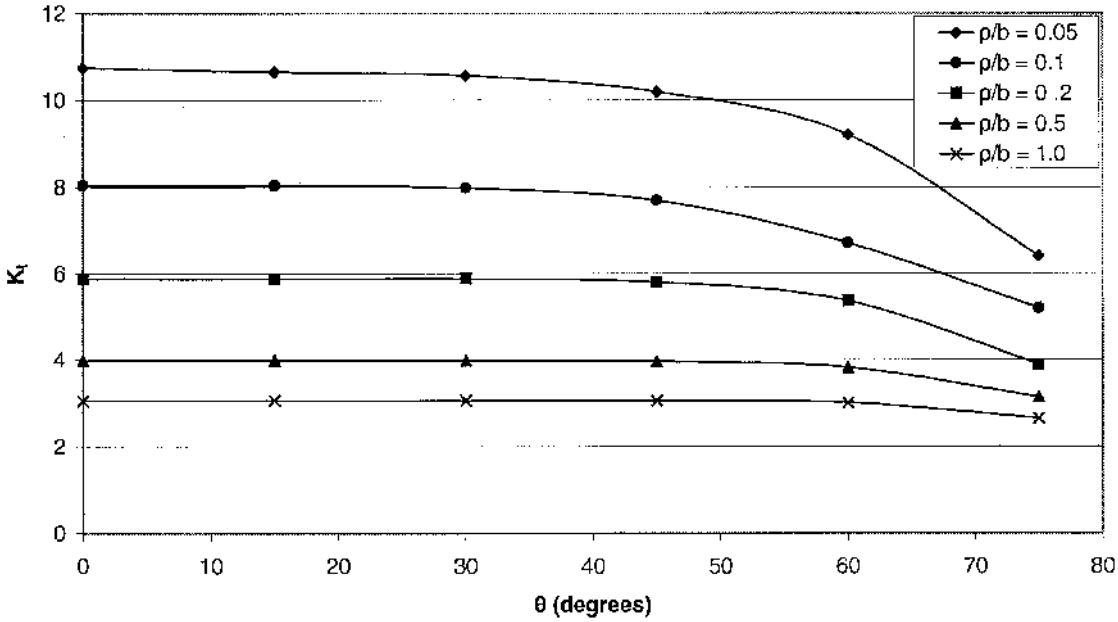

Fig. 8 Stress concentration factors for the notch, as a function of θ and ρ/b

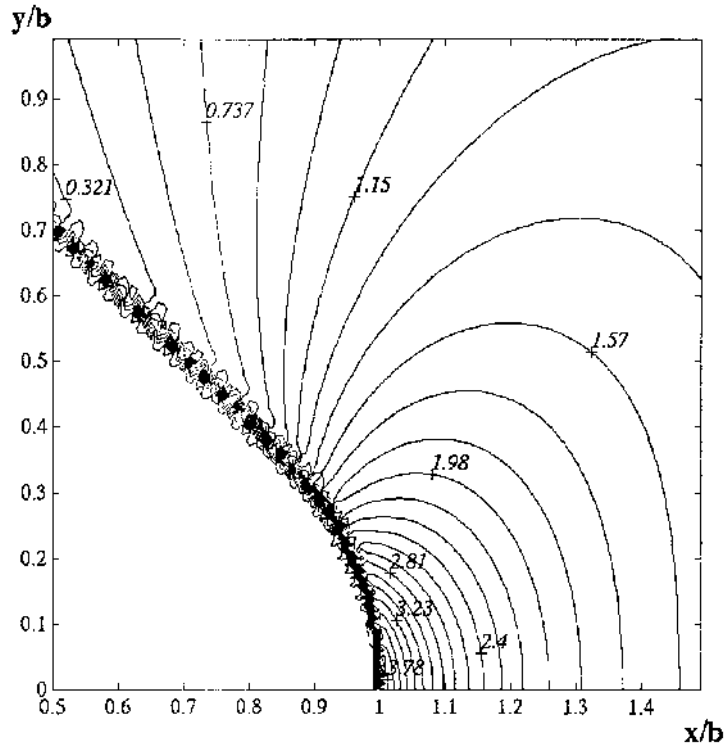

Fig. 9 Contours of σ_{yy}/σ_0 around the notch root for $\theta = 45°$ and $\rho/b = 0.5$

neighbourhood of a semi-infinite V-notch. Figure 10 shows a comparison between the results obtained from the present numerical method and the theoretical analytical solution given in reference [**16**]. It is clearly seen that, for values close to the notch tip, the solutions are almost coincident but they diverge for large values of $(x - b)/\rho$ (as shown in Fig. 10). This is clearly due to the semi-infinite assumption used in reference [**16**], where b is assumed to be infinite. Hence, the stresses depend only on $(x - b)/\rho$ and θ. The region of validity of this assumption may be found by reference to Fig. 6. Another obvious

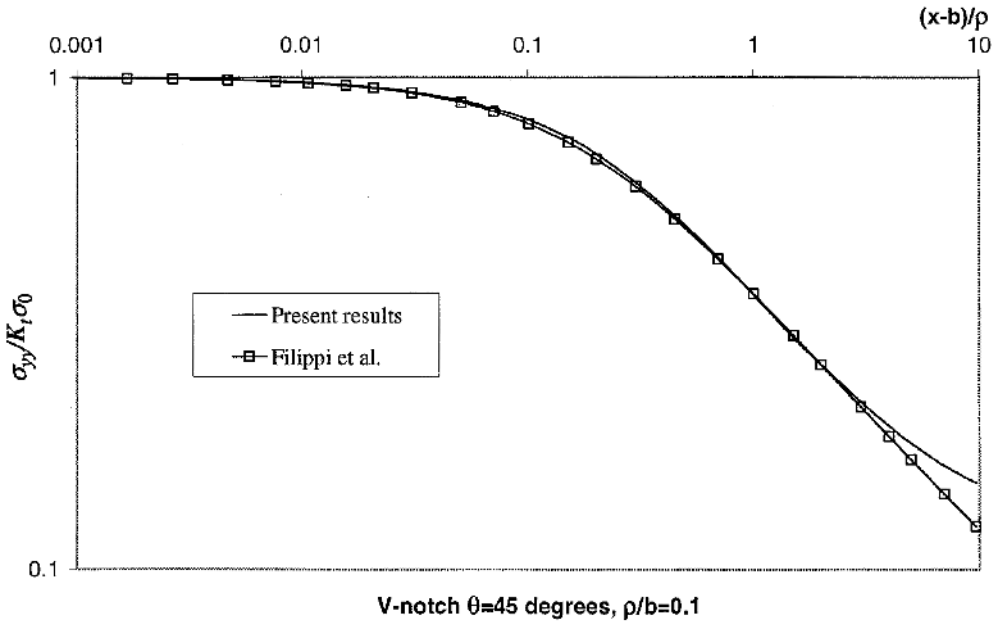

Fig. 10 Comparison of the current method with the results of Filippi *et al.* [**16**]

comparison to make is with the Creager–Paris [**17**] solution for a crack with a tip radius ρ. This may be represented in the current scheme by setting $\theta = 0$ and letting $\rho/b \to 0$. The comparison is best made by plotting the results normalized with respect to ρ, and an additional curve has been added to Fig. 6. It may be seen that, as expected, the Creager–Paris solution agrees with the present results in the region close to the notch root.

3 NOTCHES WITH CRACKS

As stated in the introduction, in the case of FOD, cracks frequently initiate at the base of the notch and these can propagate normal to the free surface under the influence of the high-cycle fatigue loading of the blade. In order to carry out fracture mechanics assessments of the possibility of crack arrest it is necessary to calculate stress intensity factors for such cracks [**3**, **5**]. The current method may readily be extended to deal with this situation. The overall geometry is now as shown in Fig. 11, where the notch is as described above and there is now a crack of length a emanating from the root of the notch. The method of solution proceeds in a similar manner to that described above. Considerations of symmetry show that the crack experiences only unsatisfied normal tractions and that only b_y dislocations are required. The existing integral equations for the notch, i.e. equations (11) and (12), need to be modified to

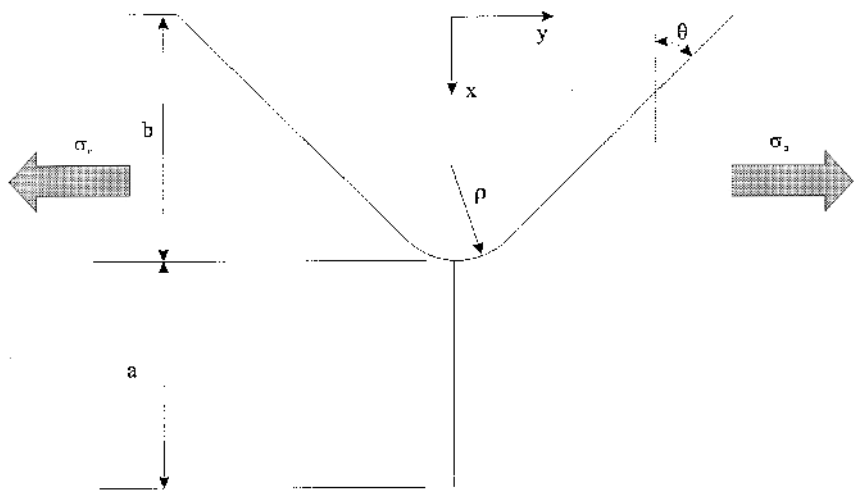

Fig. 11 V-notch with a crack emanating from the root

account for the presence of these dislocations to give

$$\frac{\pi(\kappa+1)}{\mu}\sigma_{\mathrm{NN}} + \int_0^s B_x G'_{x\,\mathrm{NN}}(x, x_\mathrm{d}, y, y_\mathrm{d}, \phi)\,\mathrm{d}t + \int_0^s B_y G'_{y\,\mathrm{NN}}(x, x_\mathrm{d}, y, y_\mathrm{d}, \phi)\,\mathrm{d}t + \int_0^a B_y G'_{y\,\mathrm{NN}}(x, x_\mathrm{d}, y, y_\mathrm{d}, \phi)\,\mathrm{d}r = 0 \tag{24}$$

and

$$\frac{\pi(\kappa+1)}{\mu}\sigma_{\mathrm{NT}} + \int_0^s B_x G'_{x\,\mathrm{NT}}(x, x_\mathrm{d}, y, y_\mathrm{d}, \phi)\,\mathrm{d}t + \int_0^s B_y G'_{y\,\mathrm{NT}}(x, x_\mathrm{d}, y, y_\mathrm{d}, \phi)\,\mathrm{d}t + \int_0^a B_y G'_{y\,\mathrm{NT}}(x, x_\mathrm{d}, y, y_\mathrm{d}, \phi)\,\mathrm{d}r = 0 \tag{25}$$

where r is an ordinate along the crack. These two equations are enforced along the notch boundary, $0 < t < s$. In addition, an additional integral equation is now enforced along the crack $0 < r < a$ to ensure that the crack faces are free of normal tractions:

$$\frac{\pi(\kappa+1)}{\mu}\sigma_0 + \int_0^s B_x G'_{x\,\mathrm{NN}}(x, x_\mathrm{d}, y, y_\mathrm{d})\,\mathrm{d}t + \int_0^s B_y G'_{y\,\mathrm{NN}}(x, x_\mathrm{d}, y, y_\mathrm{d})\,\mathrm{d}t + \int_0^a B_y G'_{y\,\mathrm{NN}}(x, x_\mathrm{d}, y, y_\mathrm{d})\,\mathrm{d}r = 0 \tag{26}$$

It is noted that symmetry requires that there are no shear tractions on the crack faces, so that a fourth integral equation to cancel these is unnecessary. Solution of these integral equations proceeds largely as outlined above. The crack exhibits a square root singularity at the tip and a singularity is also appropriate at the sharp corner where the crack meets the notch root. This requires a Gauss–Chebyshev quadrature, rather than a Gauss–Jacobi quadrature [**10**, **18**]. This uses a weight function which is singular at both ends so that

$$B_y = \Phi_y(1 - w^2)^{-0.5} \tag{27}$$

where $w = (2r - a)/a$. The quadrature scheme has N integration points, given by

$$u_i = \cos\left(\frac{(2i-1)\pi}{2N}\right), \qquad i = 1, 2, \ldots, N \tag{28}$$

and $N - 1$ collocation points

$$v_k = \cos\left(\frac{\pi k}{N}\right), \qquad k = 1, 2, \ldots, N-1 \tag{29}$$

The additional equation required to solve the problem comes from the physical requirement that the values of Φ_y on the crack and notch are matched at the corner where the crack meets the notch root. The $3N$ equations are solved as before and the stress intensity factor for the crack may be found from the value of Φ_y at the crack tip [**8**]:

$$K_\mathrm{I} = 2\sqrt{2\pi a}\,\frac{\mu}{\pi(\kappa+1)}\Phi_y(1) \tag{30}$$

Of course, Φ_y is only known at the collocation points v_k, but simple extrapolation may be employed to determine $\Phi_y(1)$. In any case, with a reasonably large value of N, the last integration point is so close to $w = 1$ that the value of Φ at the last integration point will be sufficiently accurate.

3.1 Results

Figure 12 shows the stress intensity factors obtained for $\theta = 45°$ and several different values of ρ/b as functions of crack length a/b. Also shown on the graph are two limiting conditions for short and long cracks. For short cracks, $a/b \to 0$, the crack is expected to appear as a crack at a free surface under a stress of $K_t\sigma_0$. Therefore the stress intensity factor is expected to be given by

$$K_\mathrm{I} = 1.1215 K_t \sigma_0 \sqrt{\pi a} \tag{31}$$

It may be seen that the solutions obtained do indeed approach the appropriate value for small a/b. For large a/b, the presence of the notch is expected to have limited influence and the crack–notch combination may be treated as a crack with a total length of $a + b$. Hence, the stress intensity factor will be given by

$$K_\mathrm{I} = 1.1215\sigma_0\sqrt{\pi(a+b)} \tag{32}$$

Again, it will be seen that the K_I solutions approach this value for large a/b. Indeed, the 'long-crack' solution is approached much faster than might be expected. For all the cases shown here, the long-crack solution may be seen to be a reasonable approximation for $a/b > 0.25$. For the sharper notches, the long-crack solution is approached much sooner so that, for $\rho/b = 0.05$, the long-crack solution may be used for $a/b > 0.1$. It should also be noted that the long-crack solution forms an upper bound to the solution. This is as expected, since the worst notch that can be envisaged is with $\theta = 0°$ and $\rho/b = 0$, i.e. a pre-existing crack of length b. The solutions obtained with the current method are also found to agree with those given in reference [**7**] for a

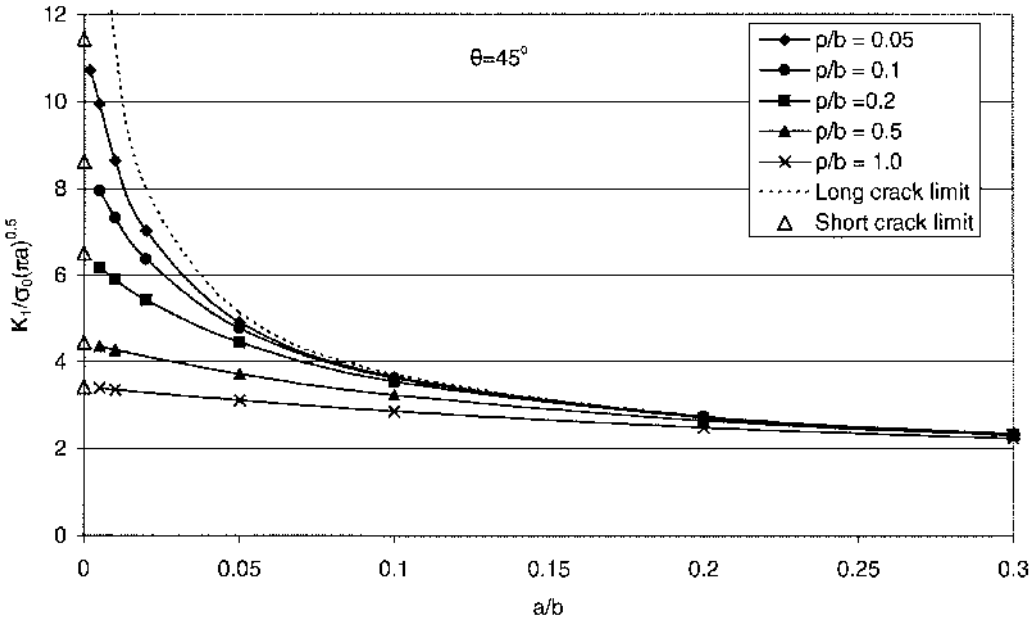

Fig. 12 Stress intensity factors for cracks emanating from a notch root ($\theta = 45°$)

crack at a sharp V-notch ($\rho/b \to 0$) and a crack at a semicircular notch ($\theta = 0$ and $\rho/b = 1$).

3.2 Residual stresses

In the FOD problem, there will be residual stresses around the notch caused by plastic deformation during the impact [**19**]. These will be important in the subsequent fatigue behaviour [**4**] and need to be incorporated in any fracture mechanics assessment [**5**]. It is therefore necessary to calculate stress intensity factors due to residual stresses as well as those caused by applied loading. The method described above may readily be adapted for a residual stress distribution $\sigma^{\mathrm{r}}_{yy}(x)$ along $y = 0$. The only difference from the case of applied loading is that the residual stress field already satisfies the requirement for zero normal and shear tractions along the notch boundary, since these surfaces are stress free after the impact. Once a crack is introduced, it will be necessary to clear the crack faces of normal tractions, and this process will cause unsatisfied tractions on the notch boundary which also need to be cleared. Hence, there will still be three integral equations to be solved, but those collocated along the notch boundary will only have the dislocation terms. Thus, the three equations become

$$\int_0^s B_x G'_{x\,\mathrm{NN}}(x, x_\mathrm{d}, y, y_\mathrm{d}, \phi)\,\mathrm{d}t + \int_0^s B_y G'_{y\,\mathrm{NN}}(x, x_\mathrm{d}, y, y_\mathrm{d}, \phi)\,\mathrm{d}t + \int_0^a B_y G'_{y\,\mathrm{NN}}(x, x_\mathrm{d}, y, y_\mathrm{d}, \phi)\,\mathrm{d}r = 0 \tag{33}$$

and

$$\int_0^s B_x G'_{x\,\mathrm{NT}}(x, x_\mathrm{d}, y, y_\mathrm{d}, \phi)\,\mathrm{d}t + \int_0^s B_y G'_{y\,\mathrm{NT}}(x, x_\mathrm{d}, y, y_\mathrm{d}, \phi)\,\mathrm{d}t + \int_0^a B_y G'_{y\,\mathrm{NT}}(x, x_\mathrm{d}, y, y_\mathrm{d}, \phi)\,\mathrm{d}r = 0 \tag{34}$$

enforced along the notch boundary, $0 < t < s$, and along the crack, $0 < r < a$, to ensure that the crack faces are free of normal tractions:

$$\frac{\pi(\kappa+1)}{\mu}\sigma^{\mathrm{r}}_{yy} + \int_0^s B_x G'_{x\,\mathrm{NN}}(x, x_\mathrm{d}, y, y_\mathrm{d})\,\mathrm{d}t + \int_0^s B_y G'_{y\,\mathrm{NN}}(x, x_\mathrm{d}, y, y_\mathrm{d})\,\mathrm{d}t + \int_0^a B_y G'_{y\,\mathrm{NN}}(x, x_\mathrm{d}, y, y_\mathrm{d})\,\mathrm{d}r = 0 \tag{35}$$

along the crack, $0 < r < a$. In any real situation, the residual stress situation will need to be obtained from simulation of the impact or from measurement. Here only some sample results for a constant tensile residual stress distribution $\sigma^{\mathrm{r}}_{yy}(x) = \text{constant} = \sigma_0$ are presented and compared with similar results for an applied stress of the same value. Results are presented in Fig. 13 for a 45° notch and $\rho/b = 0.1$ and 1.0. It will be seen that the stress-concentrating effect of the notch is almost entirely absent for the case of residual stress and that there is little difference between the two different ρ/b values. As expected, for long cracks the solutions for applied and residual stress converge, since the effect of the unloaded notch at the crack mouth becomes insignificant.

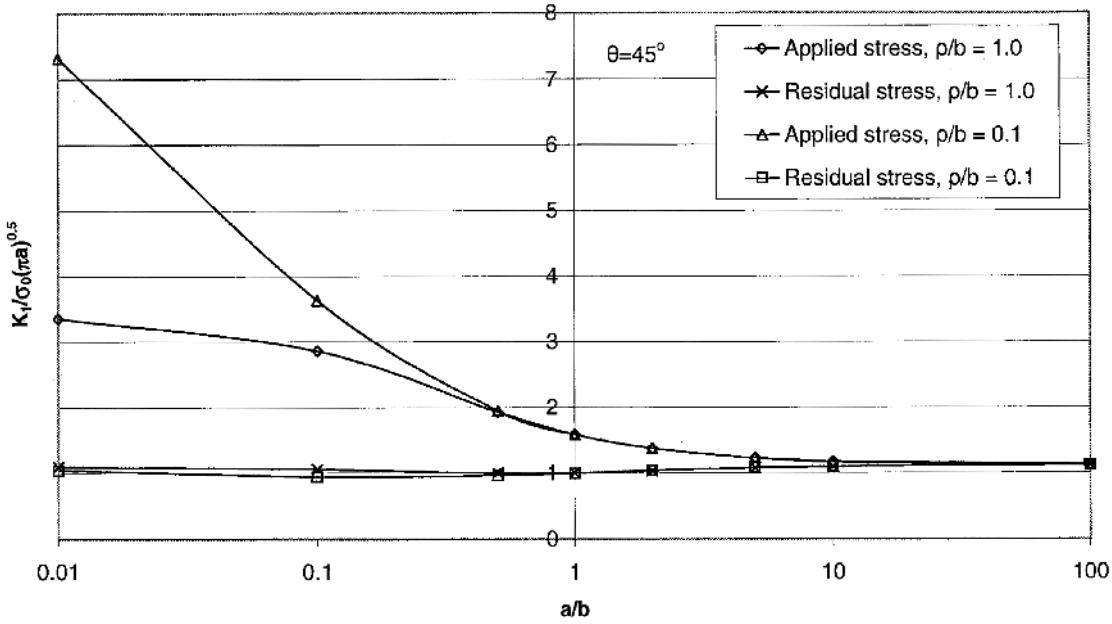

Fig. 13 Comparison of stress intensity factors evaluated for applied and residual stress ($\theta = 45°$)

However, this does not occur until the crack length is approximately ten times the notch depth.

4 CONCLUSIONS

The results presented here demonstrate that the dislocation density method is a convenient and accurate way of carrying out a two-dimensional elastic stress analysis of a V-notch with a radiused root. Notches have been analysed as features by themselves, and also with a crack emanating from the notch root. Comparisons with the classical solutions available have shown excellent agreement. For the case of a notch without a crack it has been shown that the main influence on the stress field is the notch root radius. Notch angle has very little effect on the stresses at the root for $\theta < 45°$ (i.e. where the total included notch angle is less than 90°). Stress intensity factor solutions for cracks growing from the notch root show the expected behaviour, with short cracks behaving as an edge crack under a stress field of $K_t\sigma_0$, whereas long cracks behave as a crack of total length $a + b$. The 'long-crack' solution is approached much faster than might be expected and cracks where $a > 0.25b$ may be satisfactorily approximated as an edge crack of length $a + b$ in the absence of a notch. The dislocation density method lends itself to calculation of stress intensity factors due to residual stress fields and an example result has been given. It can be seen that in this case the notch has very little effect on the solution since the concentrating effect of the notch on the stress experienced by the crack is absent.

REFERENCES

1 **Gravett, P., Bellows, R., Dunyak, T., Herrmann, D.** and **Hudak, S.** The foreign object damage program of the PRDA V HCF materials and life methods program. In Proceedings of the 4th National Turbine Engine High Cycle Fatigue Conference, Monterey, California, February 1999.

2 **Ruschau, J. J., Nicholas, T.** and **Thompson, S. R.** Influence of foreign object damage (FOD) on the fatigue life of simulated Ti–6A1–4V airfoils. *Int. J. Impact Engng*, 2001, **25**, 233–250.

3 **Nowell, D., Duo, P.** and **Stewart, I. F.** Prediction of fatigue performance in gas turbine blades after foreign object damage. *Int. J. Fatigue*, 2003 (in press).

4 **Martinez, C. M., Eylon, D., Nicholas, T., Thompson, S. R., Ruschau, J. J., Birkbeck, J.** and **Porter, W. J.** Effects of ballistic impact damage on fatigue crack initiation and early growth during high-cycle fatigue of Ti–6A1–4V. *Engng Fracture Mechanics*, 2002, **67**, 193–207.

5 **Chan, K. S., Lee, Y-D., Davidson, D. L.** and **Hudak Jr, S. J.** A fracture mechanics approach to high cycle fretting fatigue based on the worst case fret concept. I: model development. *Int. J. Fracture*, 2001, **112**(4), 299–330.

6 **Roarke, R. T.** and **Young, W. C.** *Formulas for Stress and Strain*, 1975 (McGraw-Hill, New York).

7 **Murakami, Y.** *Stress Intensity Factors Handbook*, 1987 (Pergamon, Oxford).

8 **Nowell, D.** and **Hills, D. A.** Open cracks at or near free edges. *J. Strain Analysis*, 1987, **22**(3), 177–186.

9 **Nowell, D.** Strain changes caused by finite width slots, with particular reference to residual stress measurement. *J. Strain Analysis*, 1999, **34**(4), 285–294.

10 **Hills, D. A., Nowell, D.** and **Sackfield, A.** *Mechanics of Elastic Contacts*, 1993 (Butterworth–Heinemann, Oxford).

11 Hills, D. A. and **Nowell, D.** Kinked cracks: finding stress intensity factors. In *Applied Stress Analysis* (Eds T. H. Hyde and E. Ollerton), Proceedings of the Conference on *Applied Stress Analysis*, University of Nottingham, 30–31 August 1990, pp. 36–50 (Elsevier, Amsterdam).

12 Neuber, H. *Theory of Notch Stresses*, 1958 (Springer-Verlag, Berlin).

13 Glinka, G. and **Newport, A.** Universal features of elastic notch-tip stress field. *Int. J. Fatigue*, 1987, **9**, 143–150.

14 Shin, C. S., Man, K. C. and **Wang, C. M.** A practical method to estimate the stress concentration of notches. *Int. J. Fatigue*, 1994, **16**, 242–255.

15 Lazzarin, P. and **Tovo, R.** A unified approach to the evaluation of linear elastic fields in the neighbourhood of cracks and notches. *Int. J. Fracture*, 1996, **78**, 3–19.

16 Filippi, S., Lazzarin, P. and **Tovo, R.** Development of some explicit formulas useful to describe elastic stress fields ahead of notches in plates. *Int. J. Solids Structs*, 2002, **39**, 4543–4565.

17 Creager, M. and **Paris, P. C.** Elastic field equations for blunt cracks with reference to stress corrosion cracking. *Int. J. Fracture Mechanics*, 1967, **3**, 247–252.

18 Erdogan, F., Gupta, G. D. and **Cook, T. S.** Numerical solution of singular integral equations. In *Methods of Analysis and Solutions of Crack Problems* (Ed. G. C. Sih), 1973, pp. 368–425 (Noordhoff, Leyden).

19 Peters, J. O., Boyce, B. L., Chen, X., McNaney, J. M., Hutchinson, J. W. and **Ritchie, R. O.** On the application of the Kitagawa–Takahashi diagram to foreign-object damage and high cycle fatigue. *Engng Fracture Mechanics*, 2002, **69**, 1425–1446.